Effects of annealing prior to stretching on strain induced crystallization of polyethylene terephthalate

Mélanie Girard, Christelle Combeaud, Noëlle Billon

HAL Id: hal-03499714

https://minesparis-psl.hal.science/hal-03499714

Submitted on 7 Jan 2022

Effects of annealing prior to stretching on strain induced crystallization of polyethylene terephthalate

Mélanie Girard, Christelle Combeaud**, Noëlle Billon**

* Previously at **, now at Research Center for High Performance Polymer and Composite Systems (CREPEC), Department of Chemical Engineering; and Research Center for Industrial Flow Processes (URPEI), Polytechnique Montreal, Montreal, Quebec, H3C 3A7, Canada
** MINES ParisTech, Université PSL, Centre de mise en forme des matériaux (CEMEF), CNRS UMR 7635, Sophia Antipolis, France

Abstract:

Polyethylene terephthalate (PET) is widely used in packaging and fiber industries. However, despite of its strain-induced crystallization (SIC) behavior, stretching procedures sometimes lead to dimensional instabilities upon time or at intermediate temperatures (hot filling for example). One of the solutions involves heating the sample during a specific time at a given temperature, generally after stretching, to promote more stable microstructure without endangering the texture. In this study, the effect of a light thermal treatment before stretching was explored. Herein, a study on strain-induced PET microstructure is carried out using this thermal treatment method, prior to stretching, to validate the improvement on the dimensional stability after uniaxial and biaxial stretching. While annealing leads to relaxation of any pre-organization, higher apparent crystallinity and better dimensional stability has been indeed observed after stretching using dynamic mechanical analysis and X-Ray scattering technique.

Keywords: Polyethylene terephthalate, stretching, strain induced crystallization, dimensional stability

1. Introduction

Polyethylene terephthalate (PET) is a well-known thermoplastic used for a wide range of applications where its stretchability is profitable. It presents a glass transition temperature of ca. 70˚C and a melting temperature of ca. 255˚C [1]. Because of its slow crystallization kinetics in quiescent conditions combined with a high glass transition temperature, it presents the ability to then crystallize upon stretching from its initially amorphous state. Crystals that are induced are small enough for material to remain transparent upon this strain-induced crystallization (SIC). For this asset along with good barrier properties and mechanical properties, PET is mainly used to make bottles, films or fibers. [2]

PET crystal structure is triclinic. The primitive lattice have been well-defined in the literature with $a = 4.56$Å, $b = 5.94$ Å, $c = 10.75$ Å, $\alpha = 98$ 1/2°, $\beta = 118°$, $\gamma = 112°$ [3]. If crystallized, PET X-Ray scans usually display most intense Bragg reflections for (010), ($1\bar{1}0$), (100) and ($\bar{1}05$) [4]. In this crystalline state, PET is in trans conformation.

PET repeat unit presents indeed two main conformers, i.e. "gauche" and "trans" conformations. « Trans » one is favored by stretching and cooperative interactions between unlinked trans segments can promote crystallization. Therefore, when uni- or bi-axially stretched above the glass transition temperature T_g, PET overcomes an induced crystallization when a critical draw ratio is reached. Same crystalline phase is promoted in SIC than in quiescent crystallization. However, due to differences in global chain organization, static conditions give rise to spherulites that are large enough to opacify the polymer (1 to 100 mm), whereas mechanical strain induces a smaller lamella structure without spherulitic organization keeping the transparency [5]. This second behavior is thus favored in most packaging applications. Then, the orientation level depends on the stress nature, the temperature, the strain rate, the cooling rate, and the molecular architecture. An intermediate state has been observed where the crystalline phase remains imperfect and is called the mesophase [4]. Moreover, when simultaneously biaxially stretched in equilibrated conditions, one can expect a mechanically isotropic material in the plane with an equivalent microstructure in both directions [6].

While researchers are looking for an eco-friendlier material [7, 8], a well-known remaining problem regarding PET processing is the post-processing dimensional instability [9, 10]. Polymer chains are extended during the process and residual internal stresses [11, 12] may be released with time in non-crystalline zones. Over its cycle life, the material is then submitted to such phenomenon which is enhanced by heat or pressure; it is thus especially tricky for hot-fill containers.

One way to increase crystallinity is the use of nucleating agents [13, 14]. Another solution is applying a thermal treatment or annealing after stretching. This leads to a higher nucleation and crystallization rate and hopefully less dimensional instabilities. Several patents have handled this problem and claim shrinkage reduction. Poppe et al. [15] suggest heating biaxially oriented thermoplastic resin containers using infrared radiation while introducing an inert gas to avoid collapse. For hot-fill applications above 65°C, Roberston et al. [16] have reached an enhanced stability by heating the container after stretching to increase the crystallinity leading to a higher glass transition temperature. The heat-setting procedure is widely used in fiber industry, but it also has a detrimental effect on mechanical strength.

In this work though, the idea is to treat the material before stretching, rather than after. PET samples were annealed and stretched subsequently. Following a quenching step, there were then characterized. Thus, this study consists in three stages. The first is to optimize the annealing protocol to ease the crystallization by relaxing any pre-

organization without inducing nucleation upon treatment. A stable microstructure evolution is aimed. Differential scanning calorimetry (DSC) and dynamic mechanical and thermal analysis (DMTA) were used to reach these objectives. PET treated samples were then ready to be stretched. A uniaxial stretching study was preliminary carried out to estimate the effect of annealing on the mechanical behavior during stretching and on the possible various organizations that it can lead to. These stretching conditions are indeed known to favor SIC. Characterization analyses included DMTA and wide-angle X-ray scattering (WAXS). In a third stage, once all parameters were set, biaxial tests were performed to approach the problematic encountered in film or bottle blowing industries. The viscoelastic properties and crystal definition were then followed during time for three days with DMTA and WAXS to confirm the benefit of the annealing step on the dimensional stability.

2. Methodology
   2.1. Material

The PET chosen for this study is Ramapet N180 from Indorama Ventures PCL with an intrinsic viscosity of 0.8. The stretching samples were cut in 0.8 mm-thick PET plates that have been processed by injection. Samples were extracted in flow direction and the material was isotropic.

2.2. Thermal treatment conditions

As explained in the introduction, the annealing protocol has to be optimized to reach the expected results. For this purpose, the thermal treatment conditions were defined using differential scanning calorimetry (DSC, Perkin Elmer 8000). The objective was to identify the treatment temperature and time needed to ease crystallization without developing it. As we intend to anneal the amorphous semi-product, the emphasis was placed on cold crystallization.

The DSC protocol is defined on Figure 1. After a fast heating at 200°C/min, an isothermal ramp was applied to the sample at a given temperature T, during specific time t, where T and t are the parameters of the thermal treatment which have to be defined. Then, after quenching the sample at 100°C/min down to 20°C, a linear temperature ramp was applied at 20°C/min up to 280°C to study whether cold crystallization was fastened or not. The cold crystallization enthalpy ΔH_c, the melting enthalpy ΔH_m and the crystallization temperature T_c were determined on this last ramp. For comparison purpose, an untreated sample was studied, by heating it at 20°C/min up to 280°C. The resulting parameters are referred to with a star (*) in the following. For all measurements, a precision at $\pm$ 2 J/g or 2°C was considered on the values read with the DSC.
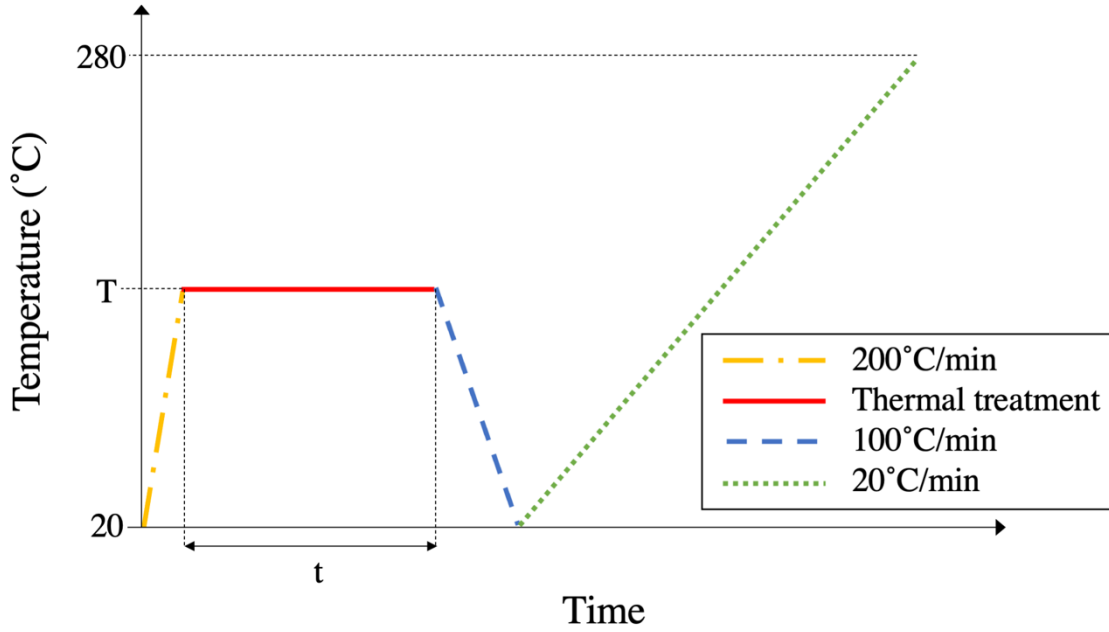
Figure 1: DSC protocol for thermal treatment parameters determination. The red line corresponds to the thermal treatment while the green line is the ramp on which the different parameters were measured.

3 requirements are considered to choose the most relevant treatment parameters:

- $\Delta H_c \geq \Delta H_c^* \neq 0$

This condition implies that no crystallization has occurred during treatment. Optic microscopy was used additionally to validate this point.

- $\Delta H_m \geq \Delta H_m^*$

Indeed, a higher crystallinity ratio (χ) is aimed, χ being defined as:

$$\chi = \frac{\Delta H_m - \Delta H_c}{\Delta H_m^*} \qquad (1)$$

- $T_c < T_c^*$

This would imply an easier crystallization due to a first initiation of cold crystallization.

Different treatment temperatures T were tested in the range of 85 to 130°C, below the cold crystallization temperature determined at 147°C at 20˚C/min. For the lowest temperatures, a longer treatment time t is needed (up to 600 s) whereas the highest temperatures were applied for a short time (as low as 6 s). However, it must be noted that any treatment time shorter than 30 s may not be feasible in real conditions and were only determined for information purpose.

It has to be noted that SIC is a different process from what the sample undergoes in the DSC machine. The resulting thermal treatment conditions had to be validated after stretching the PET sample, as explained in the part 2.4.

2.3. Dynamic mechanical and thermal analysis

Dynamic mechanical and thermal analysis (DMTA 8000, Bohlin Instruments, Perkin-Elmer) was used to characterize the PET at its initial amorphous state and to compare the stretched samples with or without treatment.

To be able to compare all samples regardless of their treatment conditions, they must be all stretched in the same physical state compared to α relaxation. However, the sample was stretched right after the annealing step using therefore the same temperature. This prevents any cooling or ageing effect. In this way, the strain rate must be adjusted accordingly (faster stretching if hotter) to analyze the material in equivalent conditions. Thus, taking advantage of classical time-temperature superposition principle, tests are referred by an equivalent strain rate $\dot{\varepsilon}_{eq}$ defined by:

$$\dot{\varepsilon}_{eq} = \dot{\varepsilon} a_{T/T_{ref}} \tag{2}$$

where $a_{T/T_{ref}}$ is the shift factor obtained with DMTA. This protocol is known to unify mechanical analysis at different temperatures and different strain rates [7, 17, 18].

The time-temperature superposition principle was applied using a reference temperature T_{ref} of 90°C. A master curve was established on the unstretched material by carrying out frequency sweeps at different temperatures, from 75 to 105°C. The tension mode was used with a dynamic amplitude of 10 μm, which induced a 3.10^{-3}-strain. The equivalent strain rate was then chosen such as the PET is in a rubbery-like state and is the same for every sample for comparison purpose.

DMTA was also used to highlight the effect of the thermal treatments. The analysis was done on the treated samples (with several treatment conditions) and compared to an untreated sample. Positive effect of the thermal treatment should increase the alpha-transition temperature (related to the glass transition) T_α, as more energy is needed to create mobility in the amorphous phase possibly constrained by the crystal. In parallel, thermal expansion or shrinkage during temperature sweeps allowed to address the dimensional stability. This was achieved thanks to the use of the "auto tension" mode that ensure that a minimal positive force is applied to the sample to avoid buckling. Tracking the associated displacement allows to estimate the thermal expansion provided that the force is low enough (1 N in our case). Consequently, all temperature sweep tests were carried out in alternate sin-tension condition at 1 Hz with a heating rate of 2°C/min and a dynamic amplitude of 10 μm. For uniaxial stretched samples, the DMTA specimen were tooled in the flow direction. It was however verified that the plaques were mechanically isotropic. For biaxial tests, samples were such as tensions were applied parallel and perpendicular to the flow direction, respectively.

2.4. Uniaxial and biaxial stretching

The uniaxial and biaxial stretching were carried out on a homemade device, illustrated in Figure 2. An air-pulsed oven can then be placed on the sample, in the center of the prototype. It was used to treat the sample before stretching. The time needed for the sample to reach T was measured around 12 s.
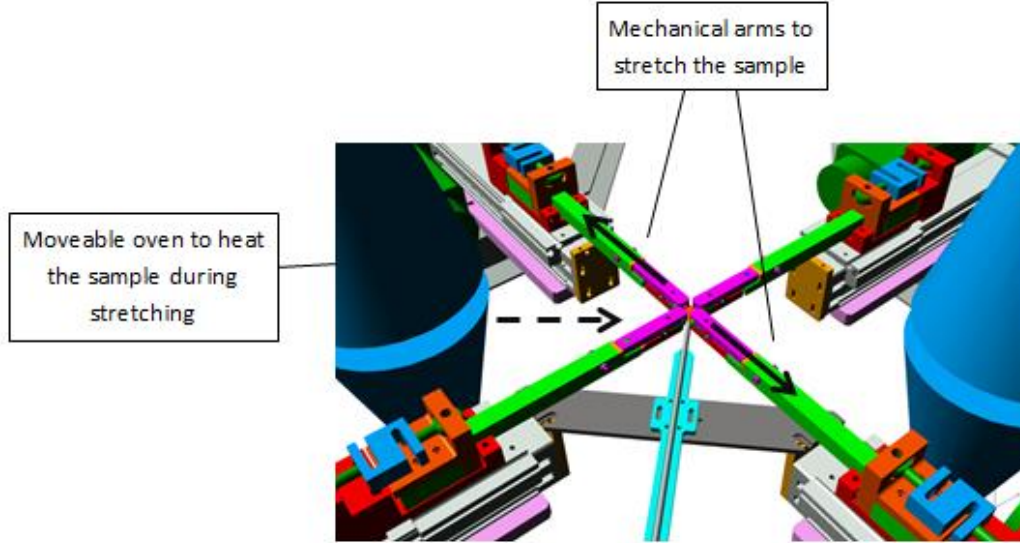

Figure 2: Stretching homemade device

Up to four independent mechanical arms can be controlled in displacement or velocity. The prototype is equipped with four independent force sensors with a capacity of 500 N, on each of the four arms. In uniaxial conditions, only one stretching direction referred as "direction 1" is used. For biaxial experiments, two stretching directions referred as "direction 1" and "direction 2" are used: simultaneous and equilibrated loadings are imposed, with the same arm velocity on each of the four arms.

The different equations related to this setup may be find in the Supplementary information. Each sample presents a final draw ratio λ_f defined by:

$$\lambda_f = \frac{l_f}{l_0} \tag{3}$$

where l_0 and l_f are respectively the initial and final process zone length for uniaxial stretching or the diagonal for biaxial stretching, where strain and stress are uniform. λ_f was determined such as the most brittle sample does not present rupture, meaning 6.25 for uniaxial and 2.6 for biaxial stretching. The final thickness deformation should be the same but with two different loadings paths, either in uni- or biaxial loading modes.

Each sample is stretched until the same strain, before being systematically air quenched. Therefore, the microstructural development involved upon stretching and post-

analyzed will depend neither on final deformation nor on cooling conditions. All these microstructural analyzes were preformed directly after stretching, with no delay.

In addition, the microstructural tests were repeated each 24 hours for three days when biaxially stretched to address the issue of dimensional stability at intermediate state.

2.5. X-ray scattering method

As the objective is to highlight a more perfected crystal and a higher crystallinity ratio, wide-angle X-ray scattering (WAXS, Phillips X'Pert PRO, Panalytical) using CuKα radiation (λ = 1.54 Å) was carried out at room temperature. Either the transmission mode (from 5° to 60°) or reflection mode (from 5° to 50°) were used. Scan intensities have been normalized by the sample thickness. Untreated samples were again compared with treated ones, just after stretching and each 24 hours for three days when biaxially stretched.

3. Results
3.1. Thermal treatment conditions

For each tested parameter, ΔH_c and ΔH_m are determined along with T_c. The results are reported in Supplementary table 1 as well as the values characterizing an untreated sample for comparison purpose (ΔH_c^*, ΔH_m^* and T_c^*). Following the method described in part 2.2, four of them fulfill the requirements and are chosen on Table 1 (bold letters in Supplementary table 1). These annealing conditions are assumed to accelerate crystallization during a subsequent heating without inducing a detectable crystallinity in the material.

Table 1: Selected thermal treatments and corresponding crystallization and melting enthalpy, crystallization temperature obtained by DSC

T (°C)	t (s)	ΔH_c (J.g^{-1})	ΔH_m (J.g^{-1})	T_c (°C)
No treatment[*]		**-27**	**27**	**147**
120	60	-26	31	136
105	180	-30	29	146
100	240	-27	27	148
95	360	-26	26	147

Thanks to DMTA, viscoelastic properties were analyzed before stretching to highlight thermal treatment effects on initial amorphous material at 105°C and 120°C which are the temperatures at which more important effects are expected (Figure 3).
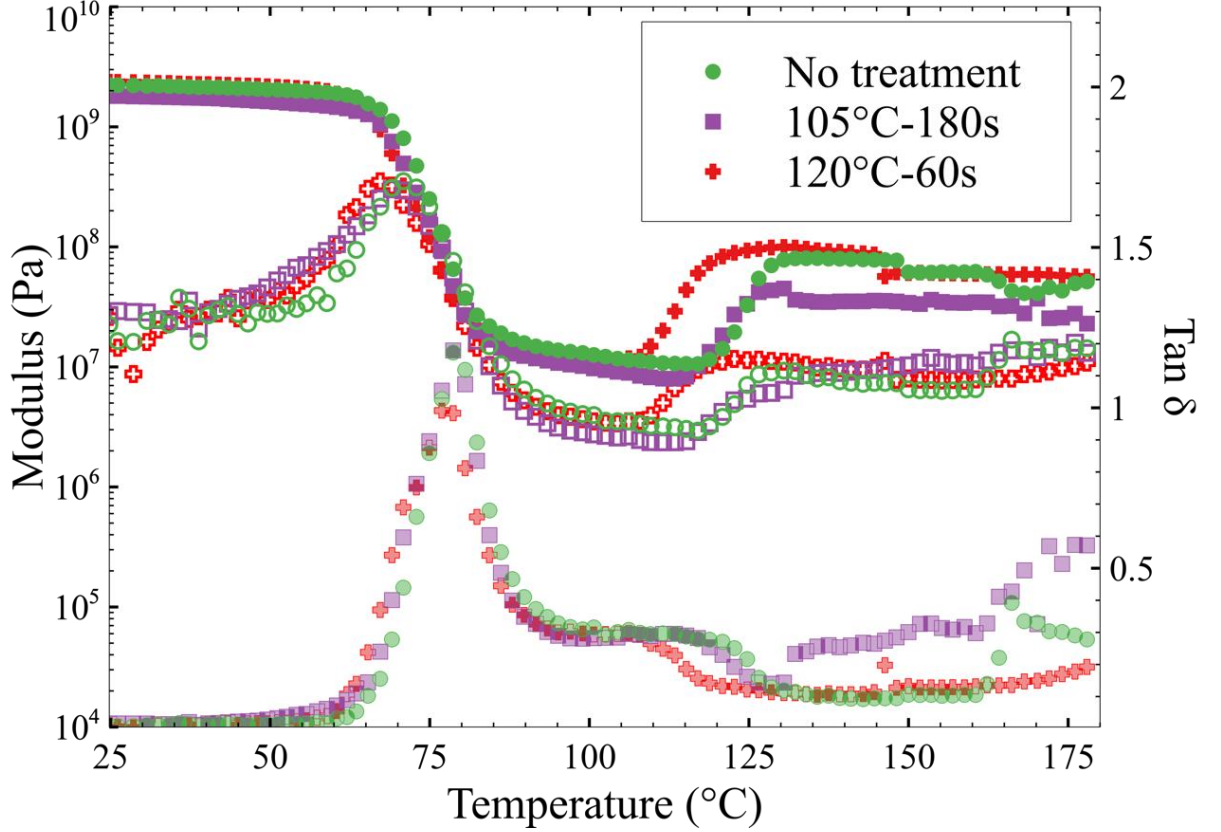
Figure 3: Storage (filled symbols) and loss moduli (open symbols) and phase angle Tan δ (hatched symbols) vs. temperature for untreated and treated samples before stretching (f = 1 Hz, heating rate = 2°C.min^{-1}, tension mode)

For all cases, alpha transition (related to glass transition) is revealed by a drastic decrease in storage modulus and a peak in loss modulus. Crystallization, for its part, results in an increase of both moduli. The treatment at 105°C seems to lead to the same response than without treatment. However, the cold crystallization offset appears at slightly lower temperature (-7°C) with the treatment at 120˚C, implying an easier phenomenon. In addition, the hottest treatment induces lower phase lag amplitude. It implies less molecular mobility in the amorphous phase without crystallinity that would have induced higher T_α.

In parallel, the X-ray scattering analysis presented in Figure 4 completes the results for the three samples showing an equivalently undetectable crystallinity. The samples remain amorphous upon treatment. It must be noted that in this figure, the hkl indexes are given to indicate where diffraction associated to crystallization should appear.
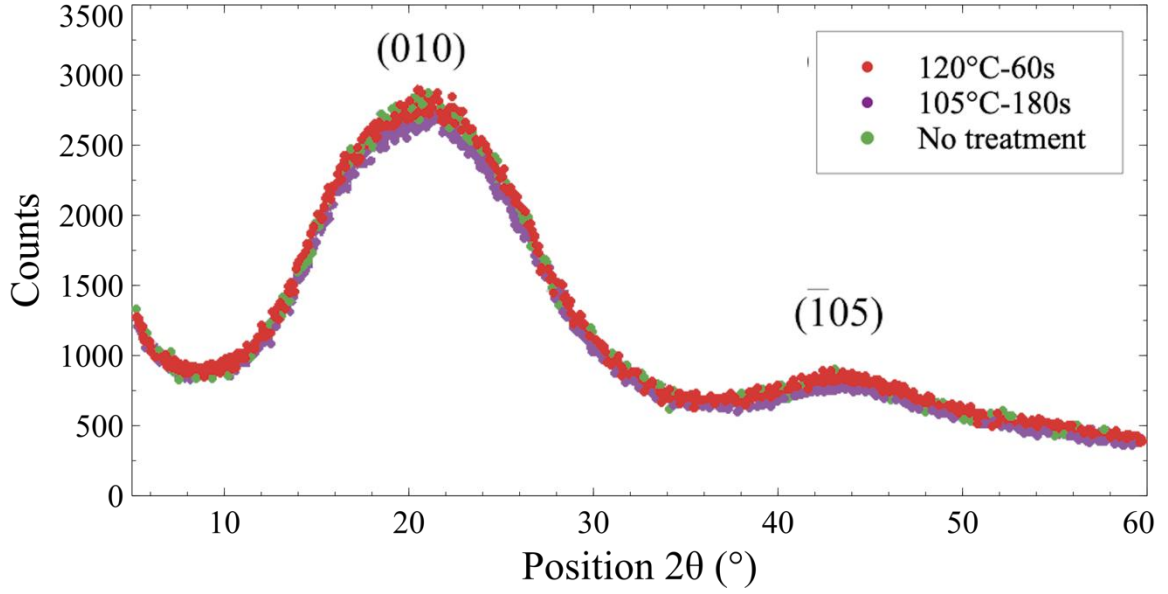
Figure 4: Wide angle X-Ray scattering diffractogram of untreated and treated samples before stretching (transmission mode)

3.2. Uniaxial stretching

Uniaxial stretching aimed at being performed in physical equivalent conditions (i.e. compared to $\alpha-$transition) but in different technological conditions (temperature T and strain rate) as explained in part 2.4.

The strain rate has been chosen regarding the PET master curve obtained by DMTA (Figure 5) as explained in part 2.3. 0.58 s^{-1} was chosen such as PET was in a rubbery-like state. This choice is clearly representative of the process parameters that will not be described in this study, for confidentiality reasons.
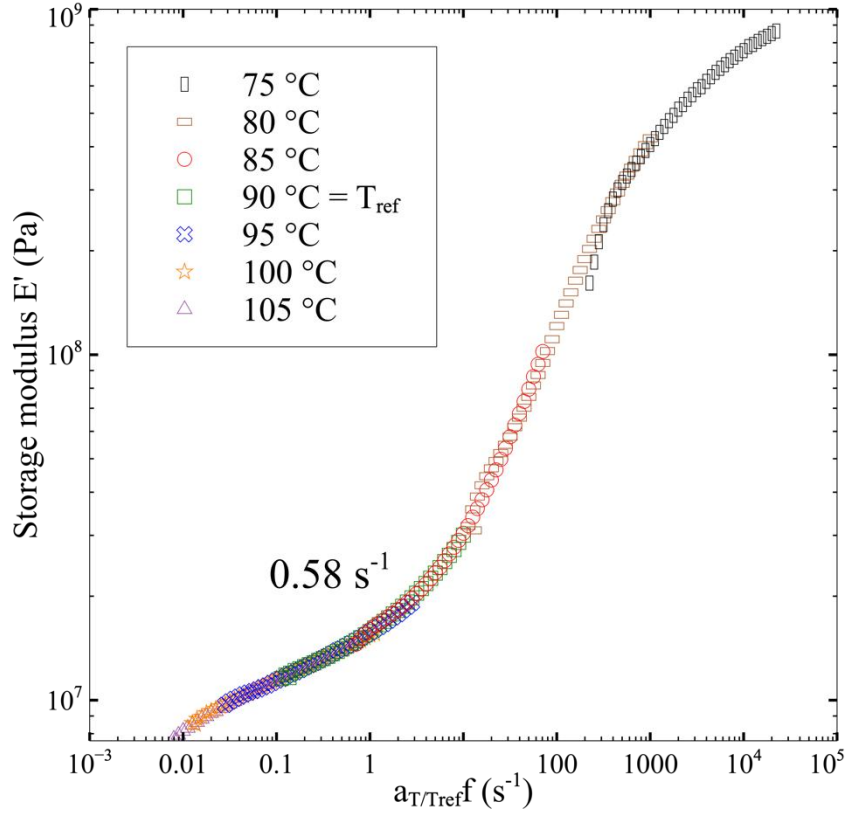
Figure 5: Storage modulus master curve at a reference temperature of 90°C for an unstretched PET sample

Accordingly, the strain rate $\dot{\varepsilon}$ at each stretching temperature must be calculated. All conditions are reported on Table 2. However, as a strain rate of 28 s^{-1} would require a too high arm velocity and possible heat dissipation, the corresponding treatment at 120 °C must be dropped.

Table 2: Uniaxial stretching parameters

t (s)	T (°C)	T$_s$ (°C)	$a_{T/T_{ref}}$	$\dot{\varepsilon}$ (s^{-1})
-	-	85	5.76	0.1
360	95	91	0.76	0.8
240	100	97	0.20	2.9
180	105	103	0.08	7.4
60	120	116	0.02	28

Using equations described in Supplementary information, it is then possible to compare true stress in function of true strain for each condition. The results are plotted in Figure 6. It must be noted that errors bars are not illustrated in this figure for readability concerns. However, when repeating the experiments, the conclusions were the same even if the reproducibility was not optimal.
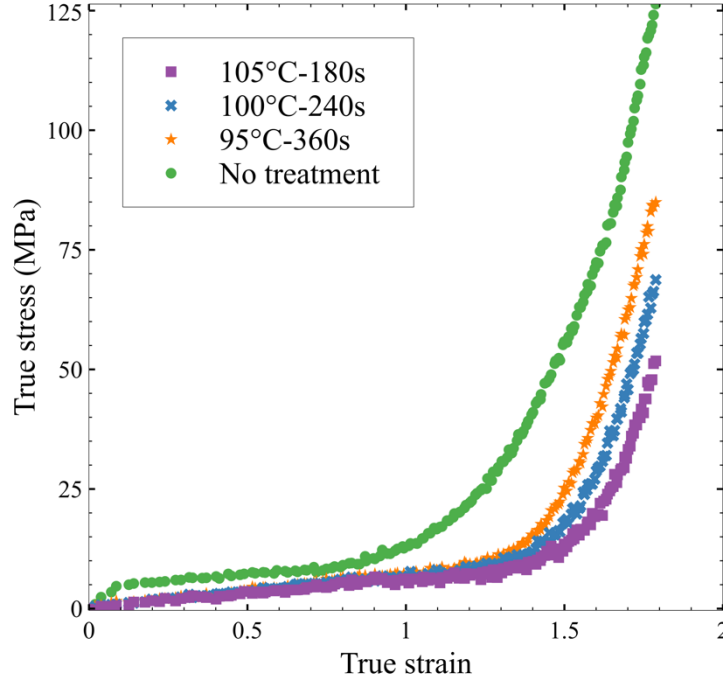
Figure 6 : True stress in function of true strain in uniaxial stretching ($\dot{\varepsilon}_{eq}$=0.58 s^{-1})

One can tempt to discuss the effect of annealing from previously reported results. It has been demonstrated that stretching amorphous polymers at a given equivalent strain rate can lead to a fixed behavior, whatever the technological conditions used (speed and temperature) [6, 18-20]. This was confirmed here as the treated samples behave the same under stretching. In addition, compared to the untreated sample, they exhibit a more clearly rubbery and less rigid behavior with a structural hardening. There is admittedly a little delay concerning the draw ratio, but it happens faster. These effects can be correlated with the very slight decrease in moduli observed in DMTA (Figure 3) on the rubbery-like plateau. These observations may suggest a microstructural state before hardening with some pre-organized zones [6, 20-23].

These zones could be at the origin of the bi-nodal scattering in its amorphous state (Figure 4) where a signature of the period ($\bar{1}$05), characteristic of the organization along the chain, persists. This organization would be responsible for the early and regular hardening of PET compared to other related polyesters (e.g. poly(ethylene 2,5-furandicarboxylate or PEF [20]). It could be destroyed by the annealing which would give the PET some additional molecular freedom and would delay the structural hardening to the moment when the crystal appears under stretching. The lower the drawing temperature, the lower the deformation. This effect cannot be attributed to a faster crystallization because if this was the case, the order would be reversed. We can therefore imagine that the residual density of "active entanglements" (i.e. after annealing) of the PET is greater during stretching at 95 °C than in the other cases. This, again, is consistent with the hypothesis of a thermally activated restructuring.

Finally, complementary analyses (DMTA and X-Ray) highlight the effect of stretching on induced microstructural developments. The storage and loss moduli E' and E'' and the loss angle Tan δ behaviors with temperature obtained in DMTA are reported in Figure 7.
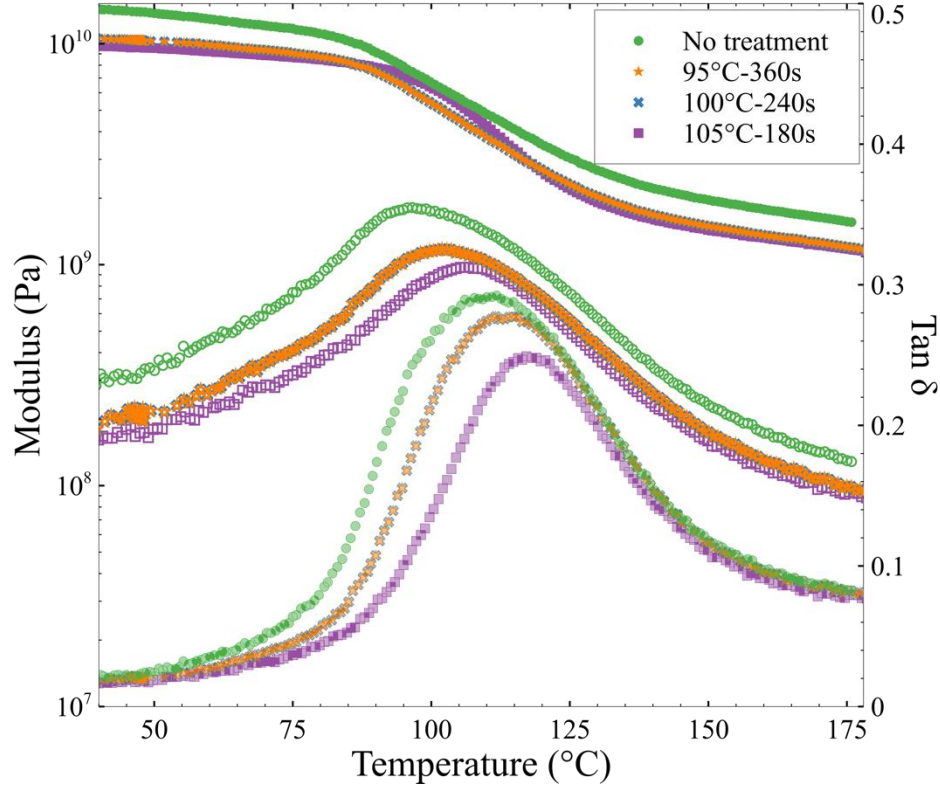

Figure 7: Storage (filled symbols) and loss (empty symbols) moduli and Tan δ (hatched symbols) for untreated and treated samples, stretched uniaxially at λ = 6.25 (f = 1 Hz, heating rate = 2°C.min^{-1}, tension mode)

One can observe that T_α increases from 108 ± 3°C to 113 ± 1°C when treating at 95°C. When increasing treatment temperature, T_α increases up to 115 ± 1°C. Note that annealing at 100 and at 105°C result in the same behavior. In addition, the α-transition happens later as the treatment temperature increases. The amorphous phase presents less mobility as highlighted by the smaller peak intensity of tan δ. Moreover, the smaller width of this peak illustrates a better homogeneity in the amorphous microstructure.

In parallel, Figure 8 depicts an important shrinkage when heated at 2°C/min. This loss of dimension stability is part of the problem we are interested in and is the trace of some restructuring of the strain induced microstructure without a clear increase in crystallinity ratio. In other word, some chain extensions are released or some mesophases are destroyed. This shrinkage is correlated to T_α and is postponed by 20 to 40°C, increasing with a higher treatment temperature. The final shrinkage values are also lower for most of

the treatments. Indeed, the pre-annealing of PET appears to be a route to reduce and postpone shrinkage of stretched part upon heating.
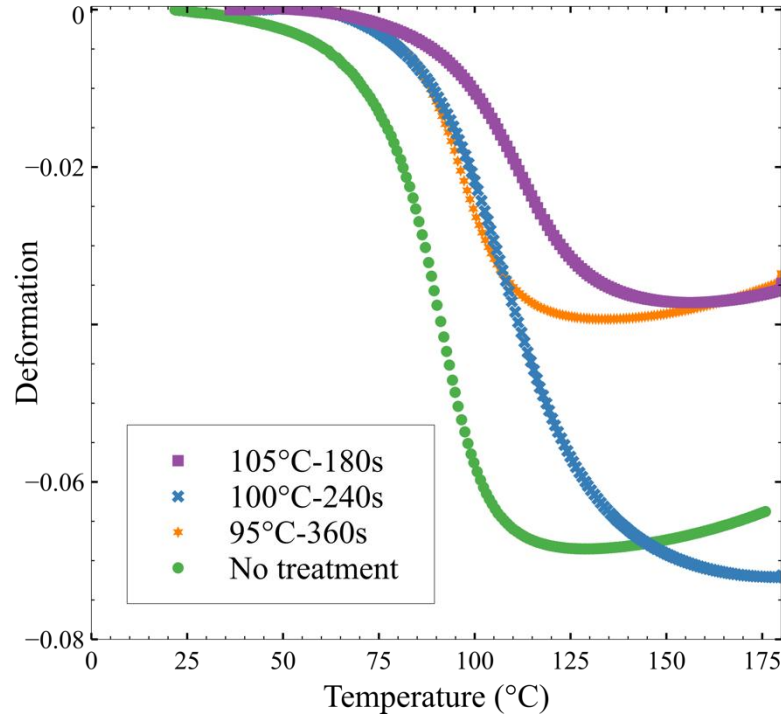

Figure 8: Thermal deformation as a function of temperature for untreated and treated samples, stretched uniaxially at $\lambda = 6.25$ (f = 1 Hz, heating rate = 2°C.min^{-1}, tension mode)

Another indirect proof is the fact that all samples stretched after annealing exhibited better-defined scattering peaks (Figure 9) with higher intensity values obtained for the treated samples. The narrower reflections for the treated samples may also imply larger crystals. This is more obvious at 105°C compared to 95°C, validating that higher treatment temperature is more efficient.
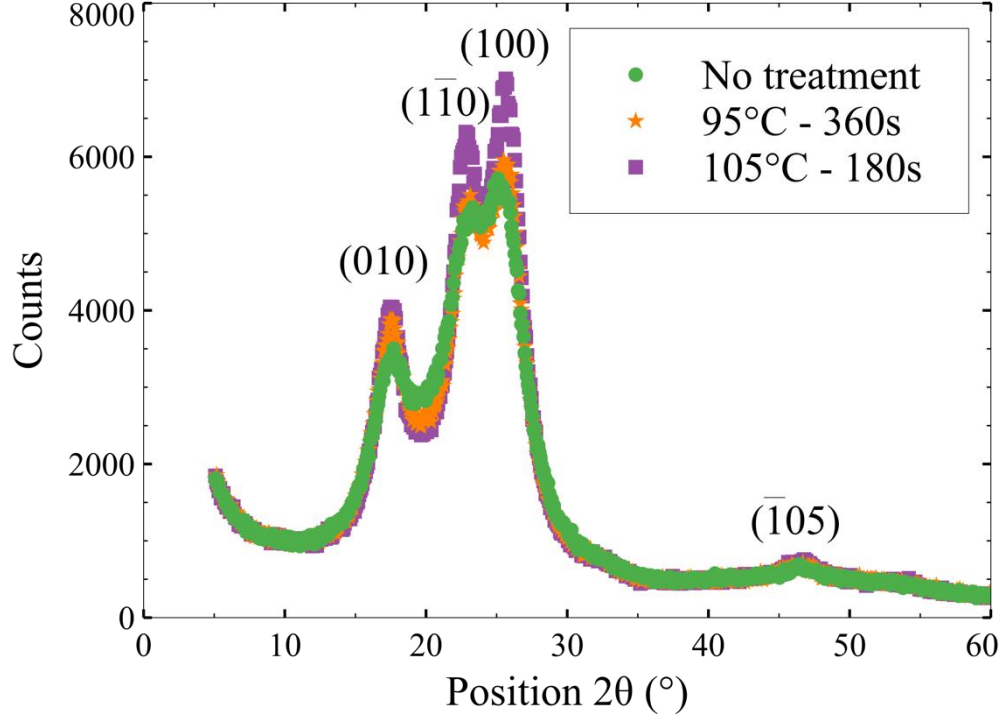
Figure 9: Wide angle X-Ray scattering diffractogram of untreated and treated samples after stretching at λ = 6.25 (transmission mode)

3.3. Biaxial stretching

Using results from uniaxial stretching, only high temperature treatments were considered. To prevent any additional temperature effect that would not be considered in the time-temperature superposition principle, a stretching temperature close to 90°C was used for all samples. The treatment at 120 °C was thus possible in biaxial stretching and could be compared with the treatment at 105°C. However, cautions need to be taken at 120°C as it is closer to the cold crystallization temperature (135 °C when heated at 10°C.min^{-1}). The treatment temperature must be reached quickly to avoid quiescent crystallization that would disturb our conclusions. Biaxial stretching parameters are reported in Table 3. As the biaxial stretching was equilibrated (same arm displacement velocity was applied from "direction 1" to "direction 2") and because the materials were mechanically isotropic, results in one direction only are presented in this part.

Table 3: Biaxial stretching parameters

t (s)	T (°C)	T$_s$ (°C)	$a_{T/T_{ref}}$	$\dot{\varepsilon}$ (s^{-1})
-	-	90	1.00	0.58
180	105	90	1.00	0.58
60	120	93	0.37	1.59

Stress-strain dependency shows no difference upon treatment (Figure 10) implying that the material behaves the same manner during stretching, with or without treatment. Once again, a slight softening is induced by annealing.
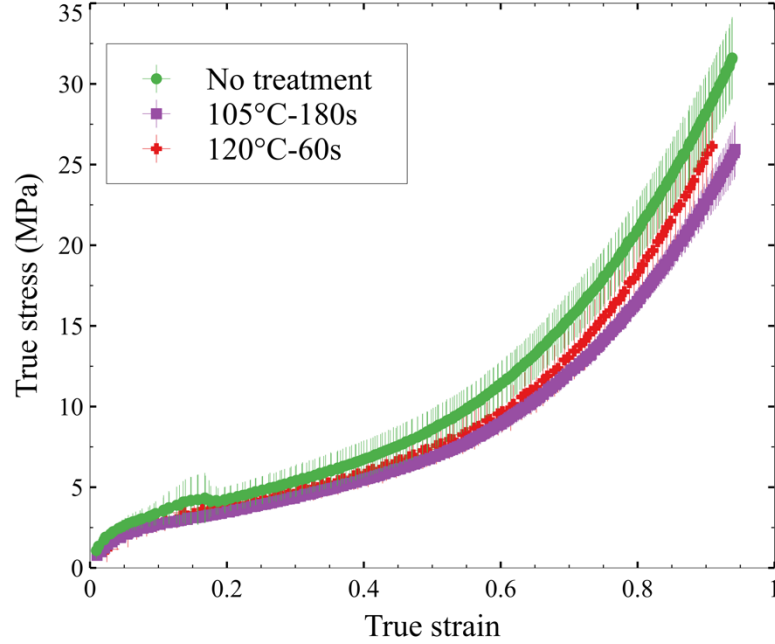

Figure 10: True stress in function of true strain in biaxial stretching ($\dot{\varepsilon}_{eq}$=0.58 s^{-1})

Figure 11 compares the sample behavior when stretched either uni- or biaxially, with or without treatment. The elastic modulus in the rubbery plateau is decreasing when the sample is stretched biaxially, suggesting a less rigid behavior and the α-transition is shifted to higher temperature. However, the intensity of tan δ peaks is lower and the width slightly larger in this case, suggesting less well-defined and more heterogeneous microstructures.
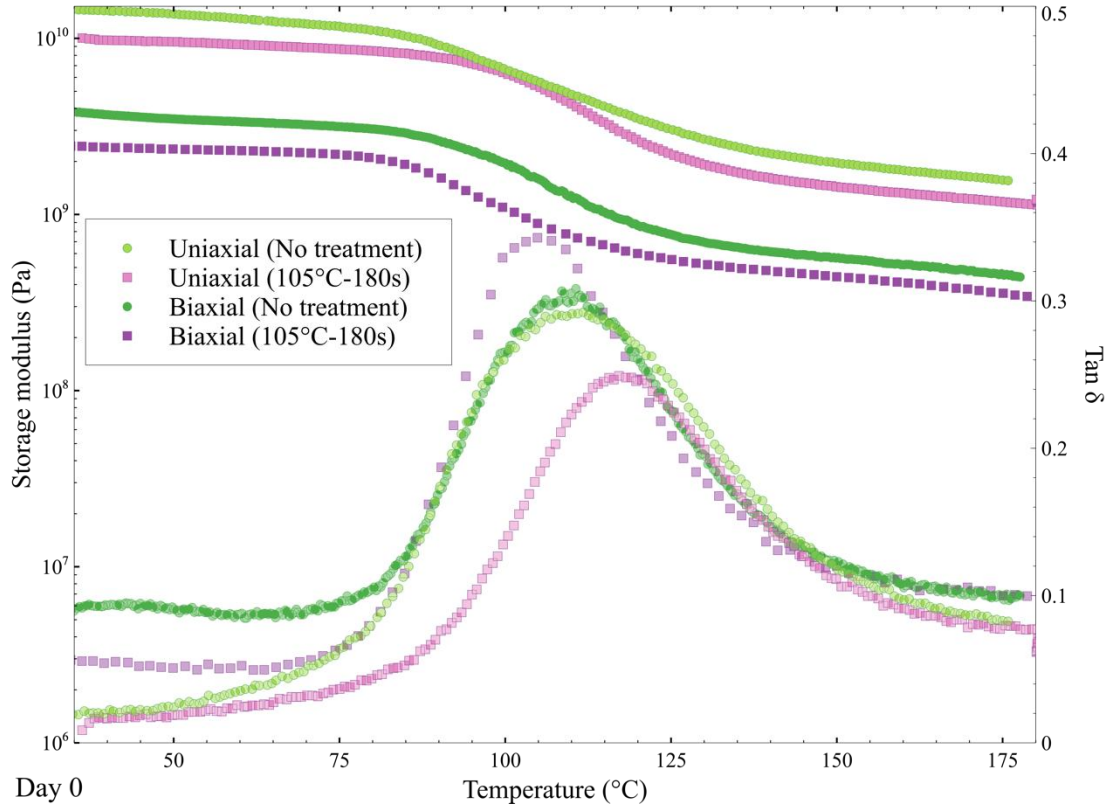
Figure 11: Storage modulus (filled symbols) and Tan δ (hatched symbols) as a function of temperature for untreated samples and samples treated at 105˚C stretched either uniaxially at $\lambda = 6.25$ or biaxially at $\lambda = 2.6$ at day 0 (f=1 Hz, heating rate=2°C.min^{-1}, tension mode) (For readability reasons, the loss modulus is not shown on this figure)

To go further, the same analyses than for uniaxial stretched samples have been repeated over time to estimate intermediate-time stability of the microstructure. It was observed that a 3-day period was necessary to reach a stable state at room temperature. The following DMTA analyses (Figure 12) present the evolution of viscoelastic properties over time, with or without pre-thermal treatment.
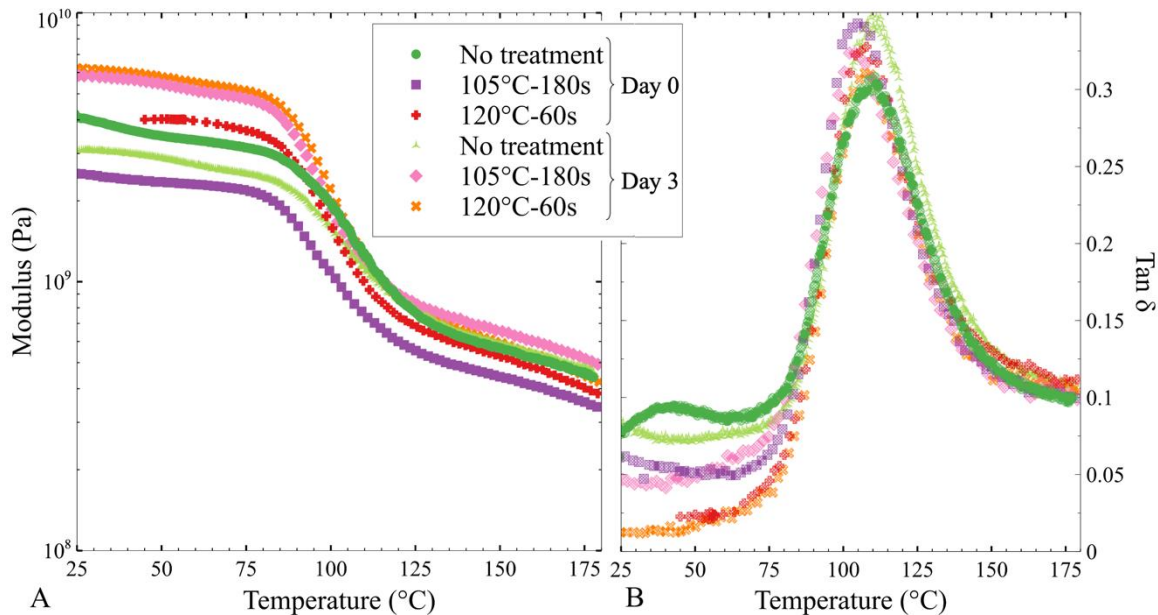
Figure 12: A) Storage modulus (filled symbols) and B) Tan δ (hatched symbols) as a function of temperature for untreated and treated samples (105°C-180s and 120°C-60s) stretched biaxially at λ = 2.6, at day 0 and day 3 (f=1 Hz, heating rate=2°C.min⁻¹, tension mode)

After 3 days, it appears that the untreated sample presents a lower glass modulus, with an evolution on the sub-glassy transition, the characteristic β-relaxation of PET. A molecular relaxation is discerned around 40°C on day 0. The associated local conformational changes are due to phenyl group oscillations or carbonyl group intensification [24]. A decrease of the β-relaxation peak temperature is observed with time. On the contrary, treated samples demonstrate a densification with increasing glass modulus over time. The secondary relaxation is never visible above 25°C when samples were pre-annealed. However, the rubbery moduli are equivalent, from a material to another. The alpha-transition is larger when treating, illustrating a more heterogeneous amorphous phase in terms of mobility. Finally, this transition happens at a lower temperature for these samples, implying a freer amorphous phase. Most of the differences are observed below T_α and should involve local changes in conformation and would be further analyzed. These figures only report results from day 0 and day 3. Intermediate date results are presented in Supplementary figure 2.

Whereas some evolution in the amorphous phase can then be suspected, there is no change with time in the crystalline phase organization as it can be concluded from the X-Ray scattering analyses (see Supplementary figure 3 for intermediate results).

The X-Ray scattering highlights better defined reflections for higher treatment temperature even if the reflection of (010) and (1$\bar{1}$0) are not visible (see Figure 13) validating the conclusions made with DMTA.
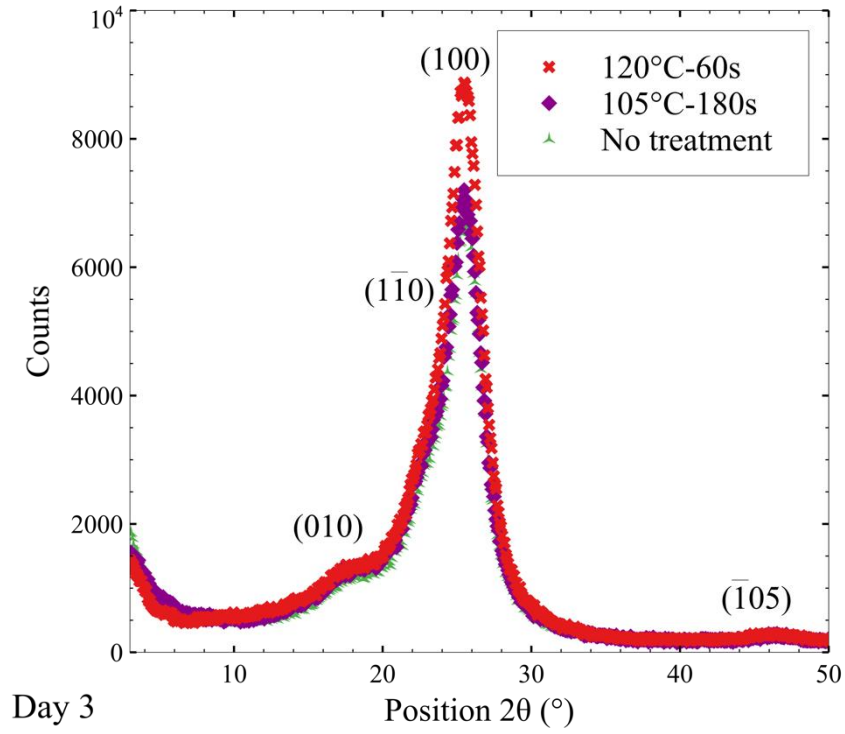
Figure 13: X-Ray scattering diffractogram of untreated and treated samples after stretching biaxially at λ = 2.6 at day 3 (reflection mode).

Eventually, the shrinkage measured at day 3 in Figure 14 validates a more stable microstructure as the treated sample does not present any shrinkage, with a better result at 120°C (see Supplementary figure 4 for results at day 0).
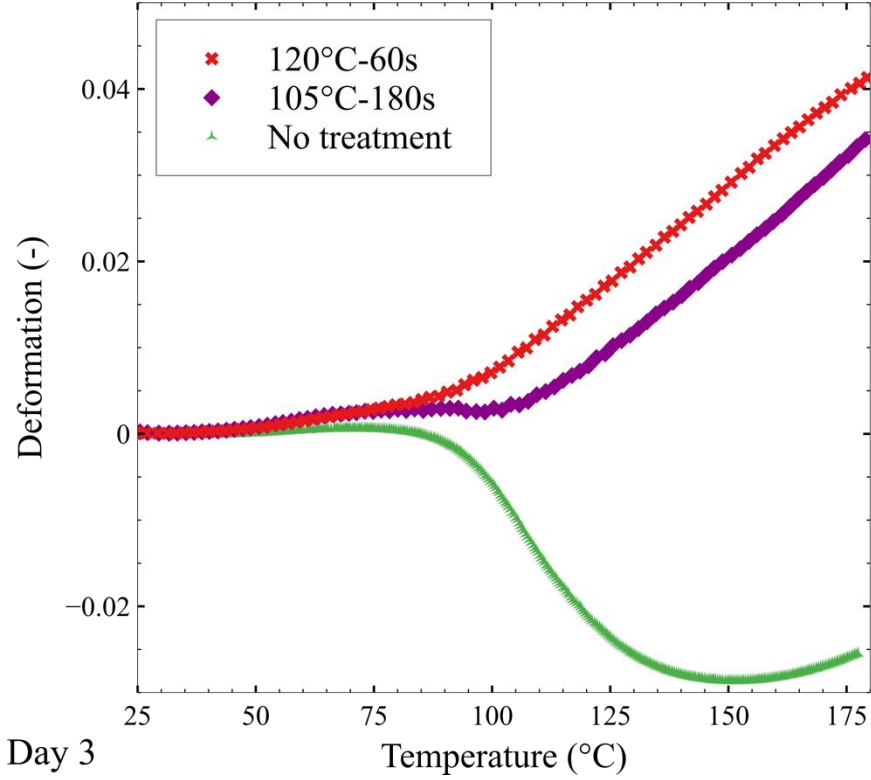
Day 3

Figure 14: Static deformation in function of temperature for untreated and treated samples stretched biaxially at $\lambda = 2.6$ at day 3 (tension test, f = 1 Hz, heating rate = 2°C.min^{-1})

4. Conclusion

This article highlights the positive effects of annealing PET prior to stretching on SIC. Indeed, uni- and bi-axial stretching tests have demonstrated that thermal treatment led to higher α-transition temperature and less shrinkage. Some schematic of the effect of annealing could be drawn suggesting a relaxation of the microstructure upon treatment. Then, the freer PET could develop higher apparent crystallinity upon SIC. The most efficient conditions are 120°C during 60s: the cold crystallization occurs at lower temperature after annealing, suggesting relaxation in the amorphous phase or nucleation point creation. After stretching, higher apparent crystallinity, elastic modulus and lower loss modulus in the glassy state are obtained. The material is thus less viscoelastic, the amorphous phase is freer, and the scattering peaks are better defined. Thus, the effect of this treatment seems to occur below glass transition temperature. Additionally, it presents a higher mechanical strength with temperature.

To deepen this study, the presence of a sub-glass transition relaxation or β-relaxation must be explored to understand its possible effect on the stretched material stability between ambient temperature and T_α. Finally, complementary results may be obtained with a calorimetric study (modulated DSC) to identify free amorphous phase and bounded amorphous phase. The stability was studied for 3 days but it would also be

interested to carry out a study on longer times (months or even years) for industrial considerations.

Supplementary information 1: equations for stretching parameters:

The estimated engineer strain rate $\dot{\varepsilon}$ is calculated using:

$$\dot{\varepsilon} \approx \frac{2v}{l_0} \qquad (S1)$$

where v corresponds to the velocity imposed on each of the arms and l_0 is the initial length of process zone for uniaxial stretching (12 mm) or the initial diagonal of central square for biaxial stretching (24 mm). Samples and their dimensions are given in Supplementary figure 1. As a reminder, the initial thickness of the specimen is approximately 0.8 mm.

True Hencky strain ε_{xx}, for both uniaxial and biaxial conditions, can be calculated such as:

$$\varepsilon_{xx}(t) = \ln \lambda(t) = \ln\left(\frac{l(t)}{l_o}\right) \qquad (S2)$$

where t is the time at which the values are taken, l(t) is the arm displacement measurement and l_0 the initial length, as mentioned in the previous paragraph.

In uniaxial conditions, the true stress may be calculated as:

$$\sigma_{T_{uni}}(t) = \frac{F(t)}{e_0 w_0 e^{2\varepsilon_{yy}(t)}} \qquad (S3)$$

where "uni" subscript stands for uniaxial stretching, F(t) is the resulting force in "direction 1", e_0 and w_0 are respectively the initial thickness and width, and $\varepsilon_{yy}(t)$ is the strain in the transverse direction.

Assuming incompressibility and transverse isotropy hypotheses, $\varepsilon_{yy}(t)$ may be defined by:

$$\varepsilon_{yy}(t) = \varepsilon_{zz}(t) = -\frac{1}{2}\varepsilon_{xx}(t) \qquad (S4)$$

The true stresses can then be defined respectively for uniaxial and biaxial conditions such as:

$$\sigma_{T_{uni}}(t) = \frac{F(t)}{e_0 w_0 e^{-\varepsilon_{xx}(t)}} \qquad (S5)$$

$$\sigma_{T_{bi}}(t) = \sqrt{2}\,\frac{F(t)}{e_0 l_0 e^{-\varepsilon_{xx}(t)}} \qquad (S6)$$

where "bi" subscript stands for biaxial stretching, F(t) is the resulting force measured in one of the two directions, e_0 and w_0 are respectively the initial thickness and width, and $\varepsilon_{yy}(t)$ is the strain in the transverse direction. As the material is supposed to be mechanically isotropic, the resulting forces measured in "direction 1" and "direction 2" are equivalent.
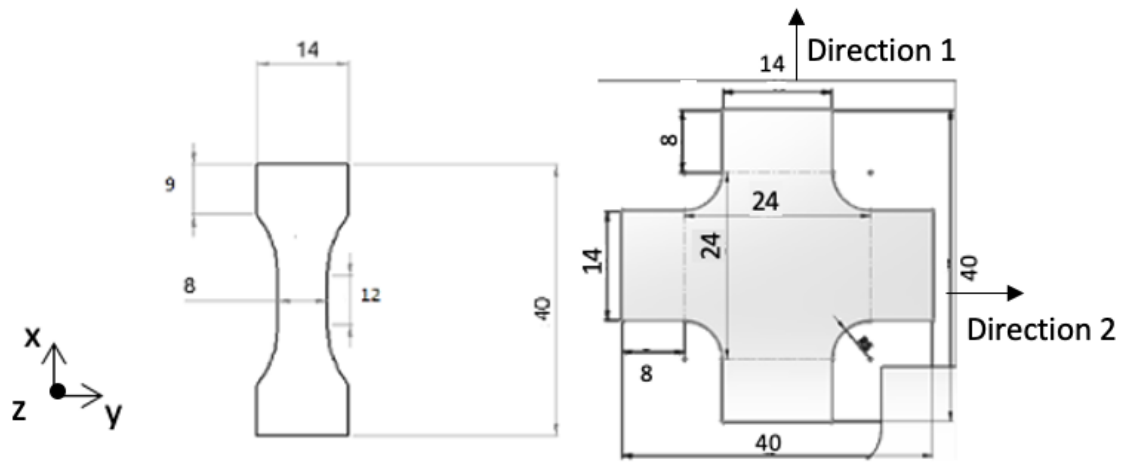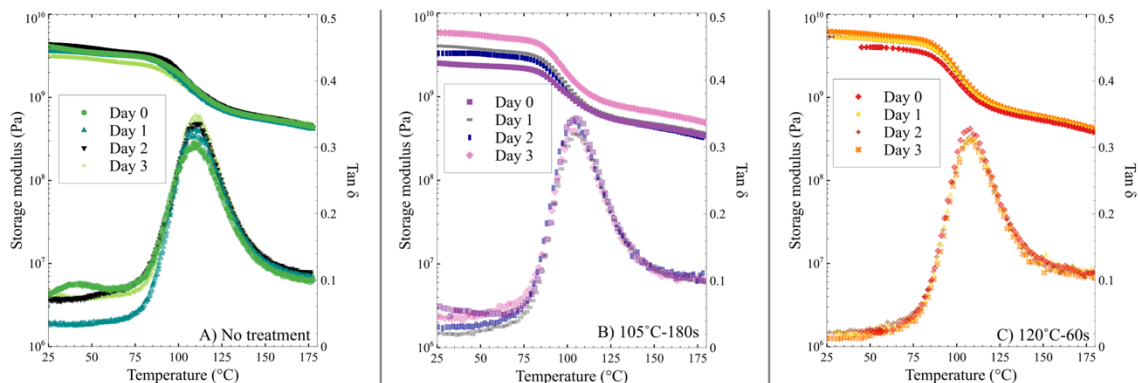
Supplementary figure 1 : Uniaxial (left) and biaxial (right) sample dimensions

Supplementary table 1 : Crystallization and melting enthalpy, crystallization temperature obtained by DSC after applying different thermal treatments

| T (°C)	t (s)	ΔH_c (J/g)	ΔH_f (J/g)	T_c (°C)
No treatment		**-27**	**27**	**147**
130	18		crystallization	
	30		crystallization	
125	18	-22	29	136
	6	-23	28	136
120	120	-17	34	136
	90	-22	30	134
	60	**-26**	**31**	**136**
	30	-18	26	135
	18	-25	28	137
	6	-22	27	137
115	120	-19	27	140
	90	-31	31	141
	60	-19	27	140
	30	-24	27	139
	18	-24	31	141
110	120	-23	30	141
	60	-24	24	148
	30	-24	28	147
105	240	-23	22	147
	180	**-30**	**29**	**146**
	120	-27	27	144
	90	-23	26	147
	60	-25	23	147
100	420	-25	25	152
	360	-29	26	146
	240	**-27**	**27**	**148**
	180	-26	25	148
95	540	-25	23	146
	480	-25	25	146
	360	**-26**	**26**	**147**
90	600	-24	25	152
	540	-27	23	149
	480	-24	25	151
85	600	-24	27	149
	540	-23	24	149

Supplementary figure 2 : Elastic (filled symbols) and tan δ (hatched symbols) in function of temperature for samples stretched biaxially at l = 2.6 from day 0 to day 3 (tension test, f = 1 Hz, heating rate = 2°C.min^{-1}). A) No treatment, B) 105˚C-180s, C) 120˚C-60s
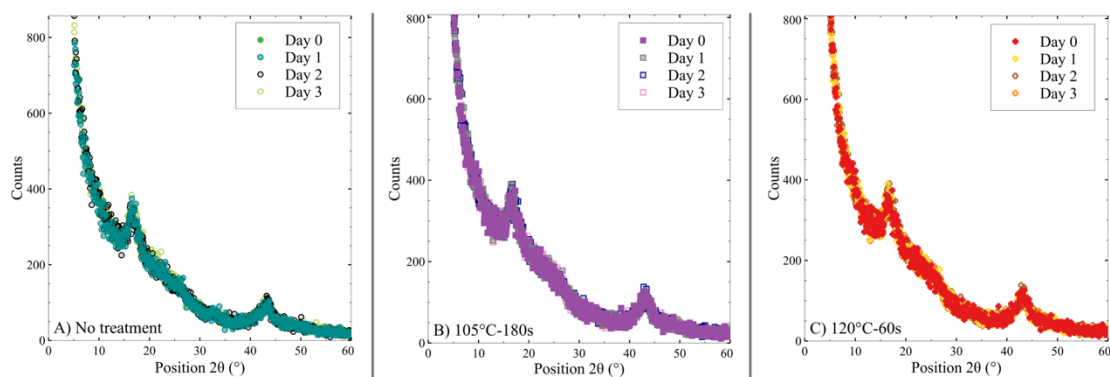
Supplementary figure 3: X-Ray scattering diffractogram of untreated sample after stretching biaxially at λ = 2.6 at day 0, day 1, day 2 and day 3 (transmission mode). A) No treatment, B) 105˚C-180s, C) 120˚C-60s
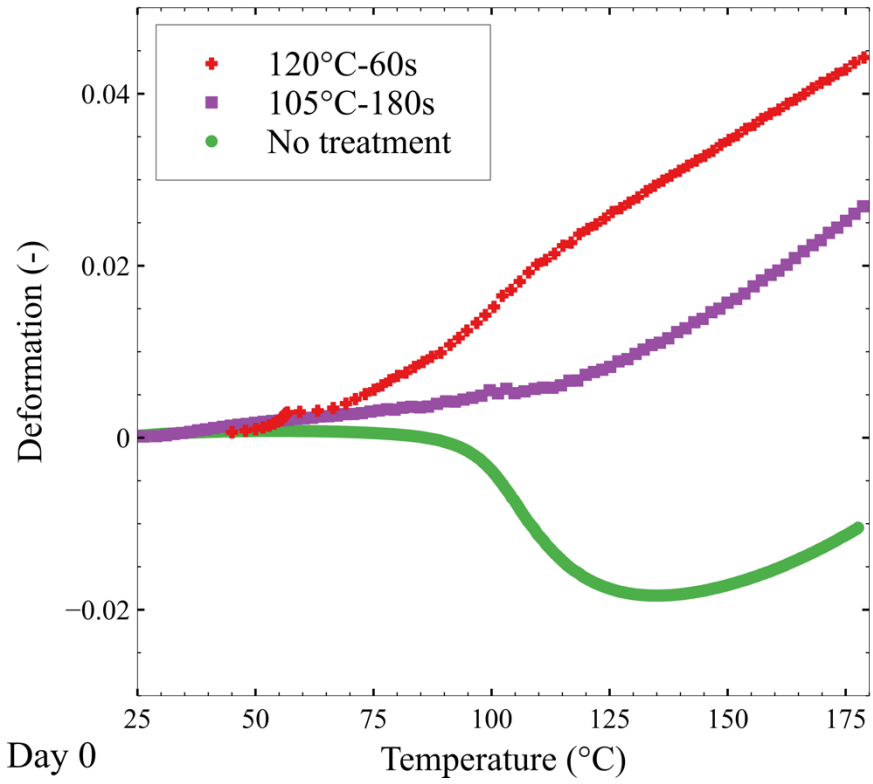
Day 0

Supplementary figure 4: Static deformation in function of temperature for untreated and treated samples stretched biaxially at $\lambda = 2.6$ at day 0 (tension test, $f = 1$ Hz, heating rate = $2°C.min^{-1}$)

[1] J. P. Jog, "Crystallization of Polyethyleneterephthalate," *Journal of Macromolecular Science, Part C: Polymer Reviews,* vol. 35, no. 3, pp. 531-553, 1995, doi: 10.1080/15321799508014598.

[2] V. B. Gupta and Z. Bashir, "PET Fibers, Films, and Bottles: Sections 1–4.13," in *Handbook of Thermoplastic Polyesters*, 2002, pp. 317-361.

[3] R. D. P. Daubeny, C. W. Bunn, and C. J. Brown, "The crystal structure of polyethylene terephthalate," *Proceedings of the Royal Society of London. Series A. Mathematical and Physical Sciences,* vol. 226, no. 1167, pp. 531-542, 1997, doi: 10.1098/rspa.1954.0273.

[4] N. Billon, M. Picard, and E. Gorlier, "Stretch blow moulding of PET; structure development and constitutive model," *International Journal of Material Forming,* vol. 7, no. 3, pp. 369-378, 2013, doi: 10.1007/s12289-013-1131-1.

[5] M. Picard, "Strain Induced Crystallisation during Stretch Blow Moulding of PET; Correlation with Strain Hardening," PhD, École Nationale Supérieure des Mines de Paris, 2008.

[6] E. Gorlier, J. M. Haudin, and N. Billon, "Strain-induced crystallisation in bulk amorphous PET under uni-axial loading," *Polymer,* vol. 42, no. 23, pp. 9541-9549, 2001, doi: 10.1016/s0032-3861(01)00497-9.

[7] E. Forestier *et al.*, "Strain-induced crystallization of poly(ethylene 2,5-furandicarboxylate). Mechanical and crystallographic analysis," *Polymer,* vol. 187, 2020, doi: 10.1016/j.polymer.2019.122126.

[8] V. Siracusa and I. Blanco, "Bio-Polyethylene (Bio-PE), Bio-Polypropylene (Bio-PP) and Bio-Poly(ethylene terephthalate) (Bio-PET): Recent Developments in Bio-Based Polymers Analogous to Petroleum-Derived Ones for Packaging and Engineering Applications," *Polymers (Basel),* vol. 12, no. 8, Jul 23 2020, doi: 10.3390/polym12081641.

[9] B. Haworth, Z. W. Dong, and P. Davidson, "Characterisation of shrinkage in oriented PET films and containers by thermomechanical analysis (TMA)," *Polymer International,* vol. 32, no. 3, pp. 325-335, 1993, doi: 10.1002/pi.4990320317.

[10] W. K. Shih, "Shrinkage modeling of polyester shrink film," *Polymer Engineering and Science,* vol. 34, no. 14, pp. 1121-1128, 1994, doi: 10.1002/pen.760341405.

[11] R. G. R. Prasath, T. Newton, and S. Danyluk, "Stress monitoring of PET beverage bottles by Digital Photoelasticity," *Manufacturing Letters,* vol. 15, pp. 9-13, 2018, doi: 10.1016/j.mfglet.2017.12.010.

[12] R. G. R. Prasath, S. Danyluk, and S. Zagarola, "Non-contact stress measurement in PET preforms," *Polymer-Plastics Technology and Materials,* vol. 58, no. 16, pp. 1802-1809, 2019, doi: 10.1080/25740881.2019.1576199.

[13] X. L. Jiang, S. J. Luo, K. Sun, and X. D. Chen, "Effect of nucleating agents on crystallization kinetics of PET," *Express Polymer Letters,* vol. 1, no. 4, pp. 245-251, 2007, doi: 10.3144/expresspolymlett.2007.37.

[14] J. Scheirs, "Additives for the Modification of Poly(Ethylene Terephthalate) to Produce Engineering-Grade Polymers," in *Modern Polyesters: Chemistry and*

Technology of Polyesters and Copolyesters, (Wiley Series in Polymer Science. Scheirs , J. ; Long, T. E. : John Wiley & Sons, Inc., 2004, ch. 14, pp. 495-540.

[15]   W. Poppe, C. F. Craddock, R. W. Gutekunst, R. G. L. Ladd, and S. A. Mager, "Shrinkage reduction of blow molded oriented pet bottle," 1981.

[16]   G. L. Robertson, *Food Packaging*, 3rd ed. 2016.

[17]   C. Menager *et al.*, "Strain induced crystallization in biobased Poly(ethylene 2,5-furandicarboxylate) (PEF); conditions for appearance and microstructure analysis," *Polymer,* vol. 158, pp. 364-371, 2018, doi: 10.1016/j.polymer.2018.10.054.

[18]   C. E. Federico, J. L. Bouvard, C. Combeaud, and N. Billon, "Large strain/time dependent mechanical behaviour of PMMAs of different chain architectures. Application of time-temperature superposition principle," *Polymer,* vol. 139, pp. 177-187, 2018, doi: 10.1016/j.polymer.2018.02.021.

[19]   F. Gehring, J.-L. Bouvard, and N. Billon, "Modeling of time dependent mechanical behavior of polymers: Comparison between amorphous and semicrystalline polyethylene terephthalate," *Journal of Applied Polymer Science,* vol. 133, no. 35, 2016, doi: 10.1002/app.43837.

[20]   E. Forestier, C. Combeaud, N. Guigo, N. Sbirrazzuoli, and N. Billon, "Understanding of strain-induced crystallization developments scenarios for polyesters: Comparison of poly(ethylene furanoate), PEF, and poly(ethylene terephthalate), PET," *Polymer,* vol. 203, 2020, doi: 10.1016/j.polymer.2020.122755.

[21]   P. L. Carr, T. M. Nicholson, and I. M. Ward, "Mesophase structures in poly(ethylene terephthalate), poly(ethylene naphthalate) and poly(ethylene naphthalate bibenzoate)," *Polymers for Advanced Technologies,* vol. 8, no. 10, pp. 592-600, 1997, doi: 10.1002/(sici)1099-1581(199710)8:10<592::Aid-pat713>3.0.Co;2-h.

[22]   A. Mahendrasingam, D. J. Blundell, A. K. Wright, V. Urban, T. Narayanan, and W. Fuller, "Observations of structure development during crystallisation of oriented poly(ethylene terephthalate)," *Polymer,* vol. 44, no. 19, pp. 5915-5925, 2003, doi: 10.1016/s0032-3861(03)00542-1.

[23]   D. J. Blundell *et al.*, "Characterization of strain-induced crystallization of poly(ethylene terephthalate) at fast draw rates using synchrotron radiation," *Polymer,* vol. 37, no. 15, pp. 3303-3311, 1996, doi: 10.1016/0032-3861(96)88476-x.

[24]   É. Deloye, "Chain architectural effect on copolyester PET behaviors during injection blow molding - Experimental study," PhD, École Nationale Supérieure des Mines de Paris, 2006.